Nonlinear local dynamics of the melt/crystal interface of a binary alloy in directional solidification

K. Tsiveriotis and R. A. Brown
Department of Chemical Engineering, Massachusetts Institute of Technology, Cambridge, Massachusetts 02139
(Received 14 June 1993)

Numerical simulations of large-amplitude cellular dynamics during thin-film, directional solidification of a succinonitrile-acetone alloy demonstrate strongly nonlinear local dynamics that involve oscillations of the deep grooves between the cells. The oscillations begin as breathing modes of the grooves and become more complex, showing period doubling, when the simultaneous dynamics of more than one groove is considered. These oscillations are not predicted by amplitude equations derived for cells near the planar interface. Simulations of the onset of cellular solidification demonstrate the importance of this mechanism to explain the scattered finite-amplitude cells that are observed in experiments near the onset of cellular solidification.

I. INTRODUCTION

Theoretical studies of the cellular patterns that form during the thin-film, directional solidification of a binary alloy continue to yield an increasing variety of nonlinear dynamics in the search for understanding of these structures. Previous studies[1–7] have explored the predictions of weakly nonlinear analyses of solidification models which are constructed by expanding in the amplitude of the cellular shape about the planar state that exists for growth rates below the critical value for the onset of morphological instability. By exploiting spatial resonance created by the lateral invariance of the cellular structure and the appearance of 2:1 resonant interactions at neutral stability, these calculations have demonstrated the occurrence of secondary bifurcations that lead to wavelength halving, traveling wave states, long time-scale oscillations, and spatiotemporal chaos. Each of these phenomena have been observed qualitatively in experiments performed with organic alloys, such as succinonitrile-acetone,[8–10] and on liquid-crystal systems,[11] although many times the depth of the experimentally observed cells is outside the range of validity of the amplitude expansions on which the analysis is based.

The purpose of this paper is to demonstrate that other, strongly nonlinear mechanisms exist for creating temporal dynamics along cellular solidification fronts and that these mechanisms play important roles in the experimental observation of cells for conditions near the neutral stability curve[10,12] and of long time-scale, chaotic dynamics.[10] The calculations reported here demonstrate the occurrence of periodic oscillations of the deep grooves between cells on a slow time scale. The oscillations cause the elongation of the grooves and are highly localized, so that the coupling between the dynamics of neighboring grooves in weak. This dynamics is strongly nonlinear, and is not captured by present amplitude analyses constructed about the planar state.

The breakup of the grooves between deep solidification cells was documented in thin-film-solidification experiments by Jackson and Hunt.[13] Brattkus[14] performed linear stability analysis on the asymptotic form for a slender groove between two cells for both two-dimensional and axisymmetric shapes to explain the break up of the groove into drops. This analysis is similar to the calculation of the linear instability of a liquid thread that is driven by surface tension and analogous results were predicted for the solidification groove: A two-dimensional groove was predicted to be always stable to small-amplitude perturbations, but the axisymmetric groove was predicted to break up with a distinct spatial wavelength along the sidewall. The wavelength corresponded well with the frequency of droplet formation seen in CBr_4 - Br_2 experiments by Kurowski *et al.*,[15] who observed droplet formation over a period of several seconds. We demonstrate below that this analysis does not capture the oscillations found in our simulations; most notably we see oscillations in two-dimensional solidification cells with periods of several hours.

The localized dynamics of grooves between cells computed here helps explain observations of Lee and co-workers[10,12] on the evolution from a planar-to-cellular interface morphology very near the onset of morphological instability. Lee and Brown observed that cellular structures are first initiated at imperfections along the interface where deep grooves form locally, followed by a much slower development of cells along the remainder of the interface. Lee and co-workers reported that the amplitude of the cells on either side of this grooves overshoots before returning to an almost steady state value at long time. We show that both of these features of the interface dynamics can be explain, at least qualitatively, in terms of the localized dynamics described here.

The solutal model for solidification and the finite-element method used for its solution are described briefly in Sec. II. Calculations reported in Section III describe time-periodic states that bifurcate from families of steady-state cells. Transient simulations of the dynamics of the transition from planar-to-cellular growth are described in Sec. IV and are compared to the observations of Lee and co-workers.[10,12]

0163-1829/93/48(18)/13495(7)/$06.00

II. SOLUTAL MODEL AND SIMULATION METHODS

The simulations reported here were carried out using the two-dimensional, two-sided solutal model for solidification, as described in other references.[7,16,17] This model includes the diffusion and convection (by the crystal translation rate) of solute through the melt and solid, segregation at the melt/crystal interface with a equilibrium partition coefficient k, and the dependence of the melting temperature on solute concentration, as modeled by a constant liquidus slope for the binary phase diagram. The effect of interfacial curvature on the melting temperature is accounted for in the Gibbs-Thompson condition for the interface. The dimensionless Gibbs-Thomson equation is reproduced here because of its importance in the dynamics described below:

$$c_{\text{ref}} + \left[\frac{G}{m}\right] y = c_m + \left[\frac{\Gamma}{m}\right] 2H \tag{1}$$

at the melt/crystal interface, where c_m is the dimensionless concentration of the melt, H is the mean curvature of the two-dimensional interface, m is the dimensionless slope of the liquidus curve of the phase diagram, G is the dimensionless capillary length, and c_{ref} is a reference concentration that is fixed at the concentration in the melt for a planar interface; i.e., $c_{\text{ref}}=1/k$. The temperature field is assumed to have a constant gradient in the direction (y) of growth and to be uniform in the direction (x) lateral to the interface; this approximation is consistent with a material with equal thermal conductivities in the melt and solid and negligible latent heat release; convective heat transport also must be insignificant. The model equations are written in dimensionless form using the wavelength of the most dangerous disturbance λ_c from linear theory as the length scale, the far-field composition c_0 as the concentration scale, the melting point of the pure material for temperature, and the time scale λ^2/D_m, where D_m is the diffusivity of the solute in the melt and λ is defined below.

Calculations are reported for samples with specified width $0 \le x \le \lambda$ and that have reflectively symmetric boundary conditions on the sides. This restriction removes the possibility of traveling-wave states from the analysis. We use the values of the dimensionless groups in the model that correspond to an alloy of 0.2 wt. % acetone in succinonitrile and a temperature gradient of 30°, or $G=4.5\times10^{-5}$ in dimensionless form, which are selected to be the same as the conditions used in the experiments of Lee and co-workers;[10,12] these parameters are listed in Refs. 7 and 13 and are not repeated completely here. However, four parameters are of particular importance, the segregation coefficient $k=0.1$, the ratio of solute diffusivity in the solid and melt, $R_m=D_s/D_m=0.05$, the dimensionless liquidus slope $m=-1.34\times10^{-3}$, and the capillary constant $\Gamma=1.9\times10^{-6}$, which scales the importance of the surface free energy in setting the melting temperature. The small value of the ratio (Γ/m) implies that the phase diagram is the dominant effect on the interface shape unless the curvature of the melt/crystal interface becomes extremely large. This effect, coupled with the poor diffusivity of the solute in the solid phase, is responsible for the creation of deep grooves between finite-amplitude cells.

The calculations use the dimensionless growth rate P as the control parameter. For the conditions used in the simulations, the critical growth rate is $P=0.0761$ at which point, sinusoidal perturbations to the planar interface with wavelength $\lambda_c=545.6$ μm are unstable; these parameters correspond to a dimensional critical velocity of $V_c=0.177$ μm/s. For these values, one unit of dimensionless time corresponds to 7.87 s.

Calculations were performed using the finite-element method with a nonorthogonal mapping that transforms the moving-boundary problem to a domain with a fixed boundary. The partial differential equations for the solute field in the melt and solid and the differential equations that describe the coordinate transformation, and hence the melt/solid interface shape, are discretized by Galerkin finite-element methods to yield a large, sparse set of differential-algebraic equations, which are integrated in time using second-order accurate backward difference approximations, with variable time steps to control solution accuracy. The finite-element meshes are created using local refinement which allows for fine resolution in regions where the interface becomes highly deformed; see Refs. 18–20 for details.

III. LOCALIZED INTERFACE DYNAMICS

Calculations were carried out for a sample size of $\lambda=\lambda_c/2$; the bifurcation diagram determined from steady-state calculations is shown as Fig. 1. The secon-

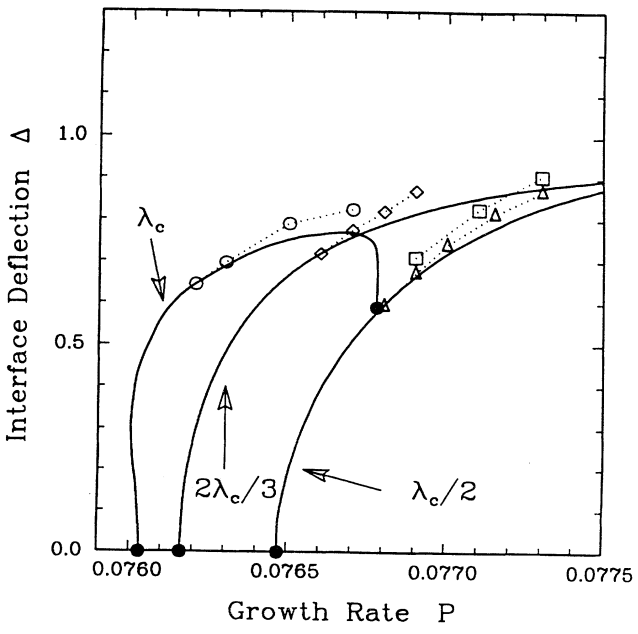

FIG. 1. Bifurcation diagram showing steady (solid curves) and time-periodic (symbols) states. Results of time dependent simulations using different sample sizes are shown as (○,□) $\lambda=\lambda_c/2$, (◇) $\lambda=\lambda_c/3$, and (△) $\lambda=\lambda_c/4$.

dary bifurcation between cells with wavelengths λ_c and $\lambda_c/2$ is apparent. Transient simulations started with the steady states in the λ_c family detected the onset of oscillatory states at $P=0.0763$, as shown by the symbols ($\circ$) in Fig. 1; this point corresponds to a Hopf bifurcation from the steady-state forms. Stable time periodic states were computed for the range $0.0763 \leq P \leq 0.0773$. An example of the time-periodic dynamics is shown in Fig. 2 by plots of the interface deflection and the interface shape as a function of time for $P=0.0767$. The oscillations are spatially localized at the grooves between the cells, which move up and down in time. This dynamics is in sharp contrast to other calculations of interfacial dynamics,[3-5,16,17] where the amplitude of the interface deflection is shallow and the dynamics involves multiple cells along the front. The localized oscillations shown in Fig. 2 hardly perturb the interface shape at the middle of the cell ($x=1$).

The distortion in the concentration field caused by the oscillation of the groove is shown in Fig. 3 for the same value of growth rate; the concentration field is plotted in the mapped variable defined as

$$c(x,y,t)=c_m(x,y,t), \text{ in the melt},$$
$$c(x,y,t)=c_s(x,y,t)/k, \text{ in the solid}, \tag{2}$$

which is continuous across the interface. During the oscillation, solute accumulates because the almost vertical walls of the groove do not facilitate segregation into the solid. The higher concentration causes the groove to deepen as the concentration increases, following the Gibbs-Thomson relationship between the melting temperature and the concentration, adjusted by the curvature of the interface. The curvature of the bottom of the groove increases as the groove lengthens, in order to compensate for the higher constitutional undercooling

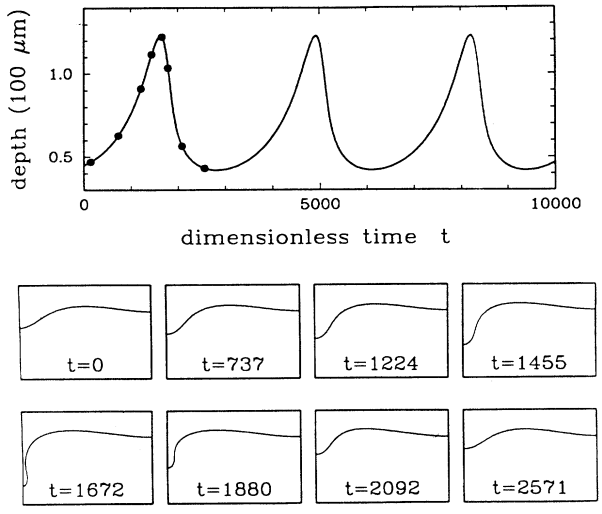

FIG. 2. Interface deflection and shape for the time-periodic oscillations computed for $P=0.0767$ and $\lambda=\lambda_c/2$. The interface shapes correspond to the points marked with (●) on the upper plot.

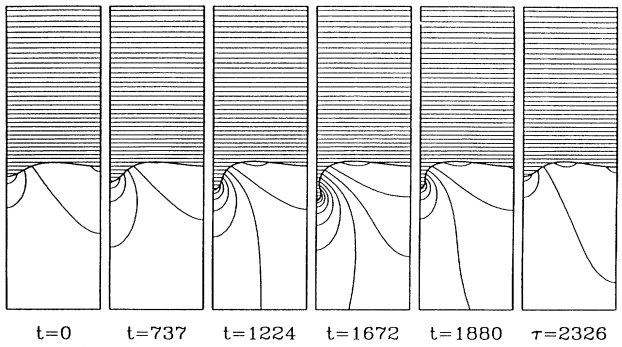

FIG. 3. Solute concentration profiles during the oscillation that develops for $P=0.0767$ and $\lambda=\lambda_c/2$, as plotted in the concentration variable given in Eq. (2).

caused by the larger concentration at the bottom of the groove. For the deepest groove, a bulbous shape results at the groove bottom which is separated from the main body of the groove by a narrow neck; this shape is characteristic of all the deep grooves seen in the localized oscillations reported here. Finally, the concentration reaches the magnitude where diffusion into the solid becomes appreciable and solute disperses into the solid adjacent to the groove. As a result, the concentration in the melt drops and the groove recoils.

Accurate approximation of the interface dynamics of the deep grooves is extremely difficult. Local refinement of the finite-element mesh in this region of the melt and solid is essential for approximating the rapid variations in curvature and concentration. The deformation of the finite-element grid during the oscillation for $P=0.0767$ and $\lambda=\lambda_c/2$ is shown in Fig. 4 to emphasize the need for the deformation of the grid into the groove as it deepens and for fine, local resolution of the interface shape. The grid shown in this figure has 40 biquadratic finite ele-

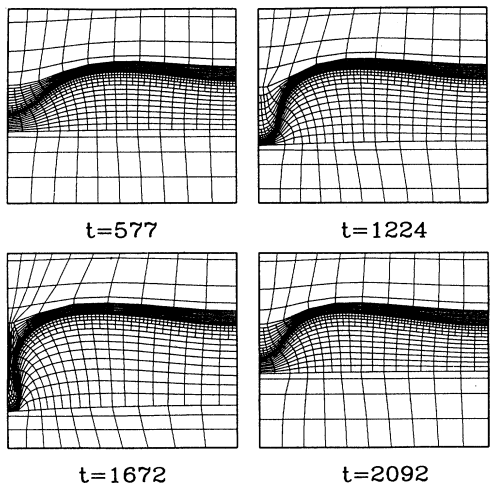

FIG. 4. Deformation of the finite-element mesh during the period of oscillation for the calculations with $P=0.0767$ and $\lambda=\lambda_c/2$.

ments distributed along the interface, representing a local refinement of a factor of 4 over the grid in the bulk melt and solid.

Because the oscillations are highly localized, increasing the number of cells in the simulation leads to the possibility of complex dynamics along the interface. This is demonstrated by calculations for growth rates P above the value $P=0.076\,78$ for the secondary bifurcation between the λ_c and $\lambda_c/2$ families of steady-state cells; as P is increased above this limit, the steady-state forms develop two cell grooves by splitting the cell tip at $x=1$. Transient simulations of the dynamics caused by initially increasing P from 0.0767 to 0.0767 78 lead to the oscillation of both grooves out of phase with each other in an apparent doubling of the dimensionless time period for the oscillation. The dimensionless period T was 3314 for $P=0.0767$ and 5768 for $P=0.0769$. This interface dynamics is portrayed in Fig. 5 for $P=0.0771$. The increase in the number of cells beyond the steady-state bifurcation point suggests that the cellular wavelength is set by tip splitting and is not affected qualitatively by the localized oscillations of the groove.

Unlike the time-periodic states that are caused by 2:1 spatial resonance,[10] the localized oscillations are relatively unaffected by the lateral size of the sample used in the calculations. To emphasize this point, we performed calculations based on sample sizes $\lambda=\lambda_c/3$ and $\lambda=\lambda_c/4$ to compute cells with wavelengths of $2\lambda_c/3$ and $\lambda_c/4$, respectively. Very similar time-periodic oscillations were computed with each of these sizes and are represented by points on Fig. 1. All the calculations involved maximum interface deflections greater than 130 μm, or 0.48 in dimensionless units. The oscillations continued to higher values of P, but the groove became too deep in the middle of the oscillation to be adequately represented by the mapping method.

Close examination of the period of the oscillation gives the strongest evidence that the oscillations are correlated with the formation of the grooves and not the cellular wavelength. The periods of the oscillations computed for all the simulations described above are plotted in Fig. 6(a) as a function of the dimensionless growth rate P. In each case, the period decreases with increasing P away from the appropriate Hopf bifurcation point $P=P_c$. According to asymptotic theory,[21] this decrease should scale as $(P-P_c)^{1/2}$. The calculations in Fig. 6(a) are consistent with this scaling. It is more interesting to replot the period as a function of the average depth of the groove during the oscillation, which corresponds to the average interface deflection; this representation is shown as Fig. 6(b). The period of the oscillation scales linearly with the groove depth. Moreover, the period of the oscillations with a single groove are highly correlated, irrespective of the sample size. The increased period for two interacting grooves is also apparent, but does not upset the linear scaling.

For the thermophysical properties of the succinonitrile-acetone system, periods between 3000 and 6000 dimensionless time units correspond to dimensional times of between 6 and 12 hours of growth. Experimental observation of these oscillations is nearly impossible, especially if one considers the complex behavior that is expected because of interactions of the grooves of neighboring cells. It is easy to image chaotic oscillations of the bottoms of a collection of grooves on very long time scales.

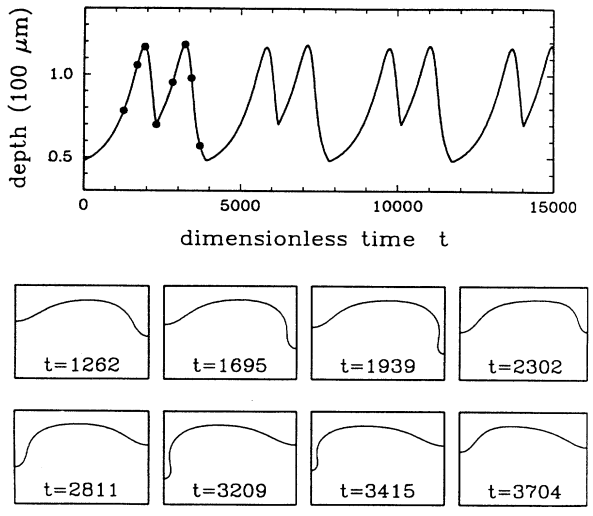

FIG. 5. Interface deflection and shape for the time-periodic oscillations computed for $P=0.0771$ and $\lambda=\lambda_c/2$ to show the period doubling caused by the dynamics of two grooves. The interface shapes correspond to the points marked with (●) on the upper plot.

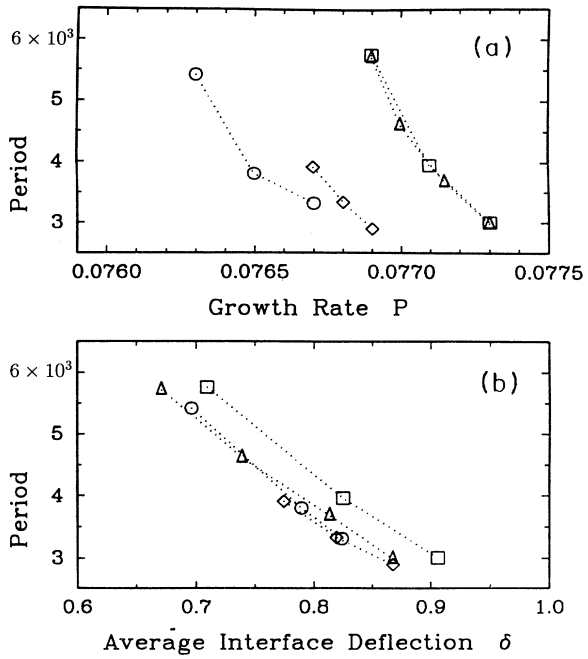

FIG. 6. Period of oscillation as a function of (a) the dimensionless solidification rate and (b) the average interface deflection over the period of the oscillation. The symbols correspond to those used in Fig. 1.

IV. DYNAMICS OF THE PLANAR-TO-CELLULAR TRANSITION

The dynamics that leads to slow oscillations of the cellular grooves also may be responsible for the observations of Lee and co-workers[10,12,22] of isolated, finite-amplitude cells along the interface just at the beginning of morphological instability. This hypothesis was tested by calculations near the planar-to-cellular transition beginning with the stable planar interface at $P=P_{\text{init}}=0.0760$ and a sample size of $\lambda=\lambda_c/3$. The solidification rate was suddenly increased at the beginning of the simulation to supercritical values of $P=P_{\text{final}}=0.0765$, 0.0767, and 0.0769. In the first simulation the interface depth increased quickly to high values before preceding through a decaying oscillation to the final, steady-state deflection predicted in Fig. 1. The time history of the interface deflection and the shape of the interface at the maximum deflection are shown in Fig. 7. For the larger two increases in the growth rate, the interface decayed into the time-periodic state involving the groove oscillation. At the largest value, the groove became too deep to be followed with the coordinate mapping technique used in these calculations, hence no dynamics is shown in Fig. 7(c) between the maximum interface deflection computed during the transient and the final time-periodic state.

An example of the overshoots in interface deflection observed by Lee[22] is shown as Fig. 8 for comparison; in this experiment the growth rate was increased from 0.67 to 0.75 μm/s and the other operating conditions were the same as those used in the calculations. As discussed in Ref. 12, the critical value for the onset of cellular solidification does not agree between the experiments and calculations, presumably because of experimental errors

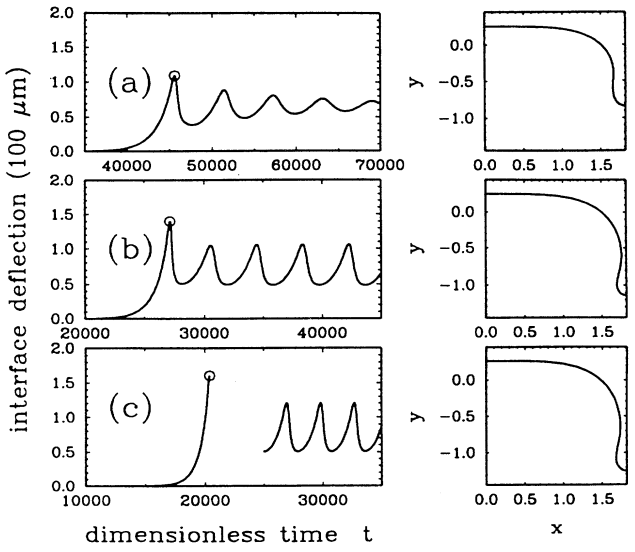

FIG. 7. Dynamics of the solidification interface after a step increase in the dimensionless growth rate from the subcritical value of $P_{\text{init}}=0.0760$ to the final value P_{final} (a) 0.0765, (b) 0.0767, and (c) 0.0769. The interface shapes at the time of maximum deflection are shown for each case.

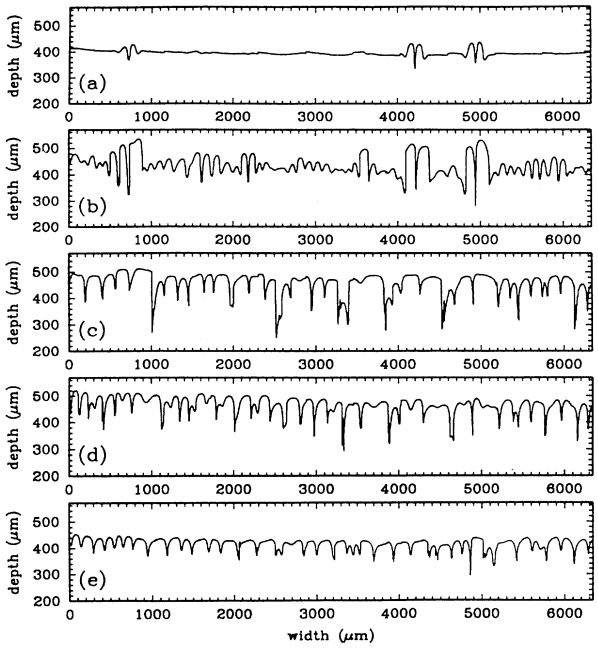

FIG. 8. Experimentally measured interface profiles for the growth of succinonitrile-acetone alloy in the thin-film solidification system described in Ref. 10, and for the same operating parameters used in the simulation shown in Fig. 6.

in the measurement of the sample concentration. The overshoot seen in the experiments associated with the localized, finite-amplitude features that develop along the interface is approximately 150 μm; these grooves reach a final depth of approximately 70 μm after 90 min. These observations compare reasonable well with the calculations of the transients caused by increasing the pull rate to $P=P_{\text{final}}$ values of 0.0765 (0.9716 μm/s) and 0.0767 (0.9741 μm/s), which exhibited overshoots of 34 and 62 μm for durations of 150 and 115 min, respectively. Here the duration of the overshoot has been defined as the time the groove spends with depths greater than the average value. The calculation with $P_{\text{final}}=0.0769$ (0.9760 μm) had an overshoot greater than 75 μm, which is the value of the deflection when the simulation was stopped. At this point the neck in the groove above the bulbous bottom had almost closed off; if it did, droplets of melt would be shed into the solid.

The similarities of the dynamics seen in the experiments and the simulations strongly suggest that the localized structures are a result of the same mechanism that leads to groove oscillations. The only remaining question is how are these structures initiated along the interface. It has long been postulated[23–25] that imperfections, such as grain boundaries, along the interface are responsible for the local nucleation of morphological instability; this hypothesis was supported by analysis using imperfect bifurcation theory[25] to show that the onset value of the growth rate for the formation of steady-state cells was singularly decreased by such an imperfection; however, the effect of imperfections on interface dynamics has not been addressed.

We have explored this coupling through a simple set of calculations in which a small, localized disturbance is introduced along the interface with the sample size $\lambda=\lambda_c$. This disturbance to the interface is expressed as $y=h(x)$:

$$h(x)=\begin{cases}-\delta\cos(2x/\lambda_c), & 0\le x\le\lambda_c/2\\ \delta, & \lambda_c/2<x\le\lambda\end{cases} \tag{3}$$

where δ is a small parameter that measures the magnitude of the initial imperfection. It is important to note that using this initial interface deflection is a much weaker perturbation to the planar state than introducing a grain boundary in the interface, which causes an imperfection that persists for all time. Condition (3) simply causes an initial perturbation that can be annealed by the dynamics which follows.

A consistent initial condition is generated for the transient simulations by solving the steady-state versions of the balance equations and mapping equations with the interface shape, Eq. (3), and $P=0.0760$, which is below the growth rate fro the onset of cell formation. The transient simulation generated from this initial state is shown in Fig. 9 for the supercritical growth rate $P=0.0769$ and $\delta=0.05$. Note that the initial indentation in the interface evolves very rapidly into a deep groove that separates moderate amplitude cells and that the remainder of the interface is barely perturbed. This simulation had to be stopped after 2063 dimensionless time units because the groove became too deep and narrow to be approximated with the coordinate mapping.

Similar calculations with $\delta=0.02$ and $P=0.0769$ are shown in Fig. 10. Again the simulations had to be terminated when the groove sidewall became so deformed that they almost touched just above the bulbous bottom; see the interface shape in Fig. 10 for $t=3413$. Note that the small-amplitude cells that are forming away from the initial perturbation have only a fraction of the amplitude of the primary indentation.

The observations in the calculations reported above are in good qualitative agreement with the dynamics seen by Lee[22] for isolated cells along an otherwise planar inter-

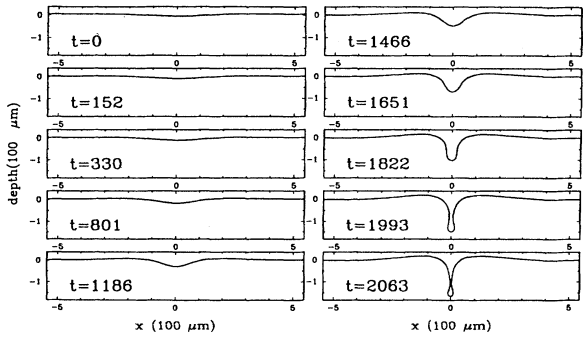

FIG. 9. Evolution of a small, localized perturbation to a planar interface as the growth rate is increased from the subcritical value of $P=0.0760$ to the supercritical value of $P=0.0769$; calculations are for $\lambda=\lambda_c$ but are plotted on the domain with $\lambda=2\lambda_c$ to facilitate comparison with experiments. The amplitude of the initial disturbance is $\delta=0.05$.

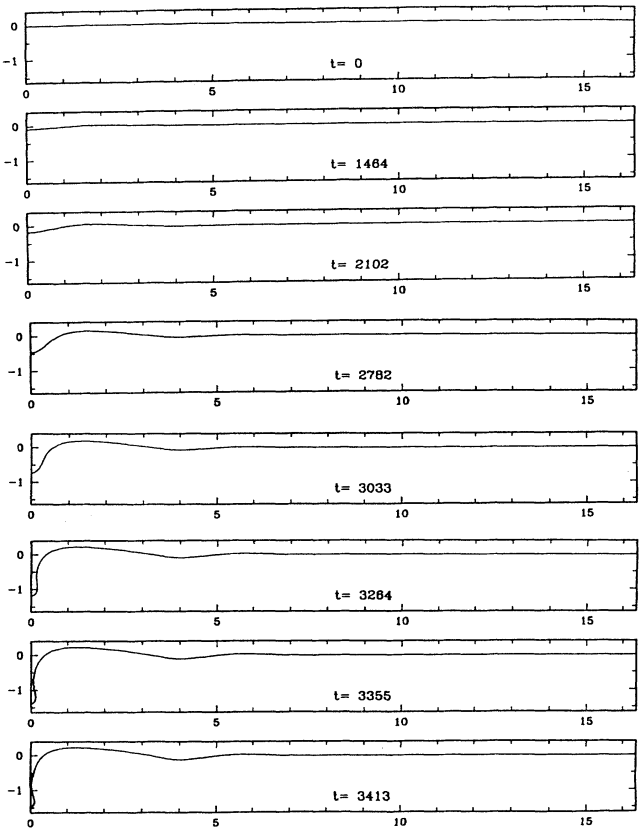

FIG. 10. Evolution of a small, localized perturbation to a planar interface as the growth rate is increased from the subcritical value of $P=0.0760$ to the supercritical value of $P=0.0769$; calculations are for $\lambda=3\lambda_c$. The amplitude of the initial disturbance is $\delta=0.02$. The scales for the abscissa and the ordinate are the same as shown in Fig. 9.

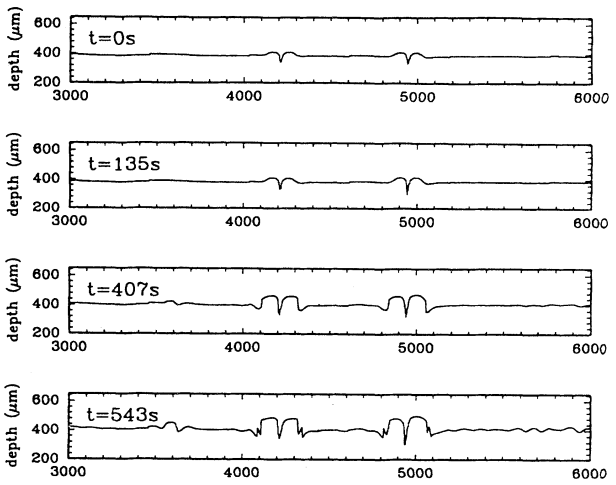

FIG. 11. Experimentally measured interface profiles for the growth of succinonitrile-acetone alloy in the thin-film solidification system described in Ref. 10, and for the same operating parameters used in the simulation shown in Figs. 7 and 8. Results are for the evolution of the interface after a step change in growth rate from 0.67 to 0.75 μm/s. The abscissa is measured in microns.

face as the growth rate is increased slightly above the critical condition. This is demonstrated by the experimentally measured interface profiles shown in Fig. 11, which is taken from the experiments of Lee for the same conditions used in the simulations, but with the defects in the interface arising from either defects in the sample container or from small-angle grain boundaries along the interface.

V. DISCUSSION

The calculations reported here described a mechanism for interface dynamics in cellular solidification that involves the localized oscillation of the grooves separating finite-amplitude solidification cells. This dynamics is due to interaction of the solute concentration field and the interface shape through the Gibbs-Thomson condition in the vicinity of the groove and is not predicted by analysis of amplitude equations developed by expanding about the planar interface shape. In the time-periodic states, the groove length oscillates up and down; when the groove is deepest, the cell bottom becomes bulbous with a narrow neck that almost pinches off to form an isolated drop of melt. This oscillation is not predicted by the linear stability analysis of the slender sidewall of a deep groove by Brattkus.[14] We expect that the surface free energy acting through the cell bottom plays an important role in the oscillation.

Weak correlation between the dynamics of multiple grooves along the solidification front leads to period doubling when two grooves are considered and, most probably, chaotic dynamics in larger collections of cells and grooves. This dynamics is predicted to occur on a very slow time scale and has not been observed yet in any thin-film solidification experiment. However, localized groove dynamics is observable in the evolution of cells from the planar state, as studied by Lee and coworkers,[10,12,22] who observed the initial formation of isolated cell pairs, separated by deep grooves and the overshoot in the amplitude of these cells with time. Both phenomena are explained by the simulations reported here for a step change in the growth rate. The overshoot in cell amplitude is a manifestation of the dynamics caused by being close in parameter space to the onset of the time-periodic groove oscillation. The initiation of cellular growth at large-amplitude, localized cells along an otherwise planar interface is explained as the transient caused by an interface imperfection, as the growth rate is increased from subcritical to supercritical values.

ACKNOWLEDGMENTS

The research described here was supported by the Microgravity Sciences and Applications Program of the National Aeronautics and Space Administration and by a grant of computer time from the Pittsburgh Supercomputer Center, which is supported by the National Science Foundation.

[1]L. H. Ungar and R. A. Brown, Phys. Rev. B **29**, 1367 (1984).
[2]L. H. Ungar and R. A. Brown, Phys. Rev. B **31**, 5931 (1985).
[3]K. Kassner and W. J. Rappel, Phys. Rev. A **42**, 7475 (1990).
[4]K. Kassner, C. Misbah, and H. Müller-Krumbhaar, Phys. Rev. Lett. **67**, 1551 (1991).
[5]A. Ghazali and C. Misbah, Phys. Rev. A **46**, 5026 (1992).
[6]A. Valance, K. Kassner, and C. Misbah, Phys. Rev. Lett. **69**, 1544 (1992).
[7]K. Tsiveriotis and R. A. Brown (unpublished).
[8]M. A. Eshelman, V Seetharaman, and R. Trivedi, Acta Metall. **36**, 1165 (1988).
[9]P. Kurowski, C. Guthmann, and S. De Cheveigne', Phys. Rev. A **42**, 7368 (1990).
[10]J. T. C. Lee and R. A. Brown, Phys. Rev. B **47**, 4937 (1993).
[11]J. Bechhoefer, P. Oswald, and A. Libchaber, Phys. Rev. A **37**, 1691 (1988).
[12]J. T. C. Lee, K. Tsiveriotis, and R. A. Brown, J. Cryst. Growth **121**, 536 (1992).
[13]K. A. Jackson and J. D. Hunt, Acta Metall. **13**, 1212 (1965).
[14]K. Brattkus, J. Phys. (Paris) **50**, 2999 (1989).
[15]P. Kurowski, S. De Cheveigne', G. Faivre, and C. Guthmann, J. Phys. (Paris) **50**, 3007 (1989).
[16]M. J. Bennett and R. A. Brown, Phys. Rev. B **39**, 11 705 (1989).
[17]M. J. Bennett, K. Tsiveriotis, and R. A. Brown, Phys. Rev. B **45**, 9562 (1992).
[18]K. Tsiveriotis and R. A. Brown, Int. J. Numer. Methods Fluids **14**, 981 (1992).
[19]K. Tsiveriotis and R. A. Brown, Int. J. Numer. Methods **16**, 827 (1993).
[20]K. Tsiveriotis, Ph.D. thesis, Massachusetts Institute of Technology, Cambridge, 1992.
[21]G. Iooss and D. D. Joseph, *Elementary Stability and Bifurcation Theory,* 2nd ed. (Springer-Verlag, Berlin, 1990).
[22]J. T. C. Lee, Ph. D. thesis, Massachusetts Institute of Technology, 1991.
[23]L. R. Morris and W. C. Winegard, J. Cryst. Growth **5**, 361 (1969).
[24]R. J. Schaefer and M. E. Glicksman, Metall. Trans. **1**, 1873 (1970).
[25]L. H. Ungar and R. A. Brown, Phys. Rev. B **30**, 3993 (1984).